Hindawi Publishing Corporation
International Journal of Rotating Machinery
Volume 2007, Article ID 34752, 10 pages
doi:10.1155/2007/34752

Research Article

Numerical Investigation on Pressure Fluctuations for Different Configurations of Vaned Diffuser Pumps

Jianjun Feng, Friedrich-Karl Benra, and Hans Josef Dohmen

Department of Mechanical Engineering, Faculty of Engineering, University of Duisburg-Essen, 47048 Duisburg, Germany

Received 3 June 2006; Revised 8 December 2006; Accepted 16 January 2007

Recommended by Shimpei Mizuki

Numerical simulations on impeller-diffuser interactions in radial diffuser pumps are conducted to investigate the unsteady flow, and more attention is paid to pressure fluctuations on the blade and vane surfaces. Calculations are performed at different operating points, different blade number configurations, and different radial gaps between the impeller and diffuser to examine their effects on the unsteady flow. Computational results show that a jet-wake flow structure is observed at the impeller outlet. The biggest pressure fluctuation on the blade is found to occur at the impeller trailing edge, on the pressure side near the impeller trailing edge, and at the diffuser vane leading edge, independent of the flow rate, radial gap, and blade number configuration. All of the flow rate, blade number configuration, and radial gap influence significantly the pressure fluctuation and associated unsteady effects in the diffuser pumps.

1. INTRODUCTION

The flow in avaned diffuser pump is dominated by strongly unsteady interactions due to the relative motion and close proximity between the rotating impeller and stationary diffuser, known as impeller-diffuser interactions, resulting in pressure and velocity fluctuations both upstream and downstream. Some research work was conducted to investigate impeller-diffuser interactions both numerically and experimentally. LDV (laser Doppler velocimetry) and PIV (particle image velocimetry) were applied to measure the unsteady flow field. Here important work was done for example by Hajem et al. [1], Akhras et al. [2], Sinha et al. [3, 4], and Wuibaut et al. [5]. Some other work was performed to study the pressure fluctuations in the diffuser region. For example, Qin and Tsukamoto [6] calculated pressure fluctuations in the diffuser region by a two-dimensional singularity method. Wang and Tsukamoto [7, 8] developed a two-dimensional vortex method to investigate pressure fluctuations both in the impeller and diffuser regions. Shi and Tsukamoto [9] studied pressure fluctuations in the diffuser region by a CFD code STAR-CD. Furthermore, experiments were conducted to measure pressure fluctuations in diffuser radial pumps by Arndt et al. [10, 11], Furukawa et al. [12], Guo and Maruta [13]. All the above-mentioned experimental and numerical investigations contribute to a better understanding of impeller-diffuser interactions in radial diffuser pumps; however the study is still not sufficient; particularly, most research on the unsteady pressure fluctuation has been conducted only in the diffuser region, but less for the impeller region.

This paper focuses on the unsteady phenomena induced by impeller-diffuser interactions in radial diffuser pumps. The pressure and velocity fluctuations and also associated unsteady effects are numerically investigated under different flow rates, radial gaps, and blade number configurations by using the CFD code CFX-10 [14]. Numerical results for different cases are compared and discussed in detail, in order to enhance the comprehension of impeller-diffuser interactions in radial diffuser pumps.

2. GEOMETRY AND GRID GENERATION

The test pump stage consists of an impeller, a vaned diffuser, and a vaned return channel. The impeller is shrouded with six two-dimensional and strongly backswept blades, with an exit angle of 22.5 deg relative to the tangential direction. The radial gap between the impeller outlet and diffuser inlet is 3% of the impeller outlet radius. Both the diffuser and return channel have nine two-dimensional vanes. All the blades are designed in two dimensions with a constant thickness of

Table 1: Specifications of the pump stage.

Impeller			*Return channel*		
Number of blades	Z_i	6	Number of vanes	Z_r	9
Inlet radius	R_1	40 mm	Inlet radius	R_5	95 mm
Outlet radius	R_2	75.25 mm	Outlet radius	R_6	50 mm
Blade height	b_i	12.7 mm	Vane height	b_r	14 mm
Front-side chamber height	h_{fs}	1.85 mm	—	—	—
Back-side chamber height	h_{bs}	2 mm	—	—	—
Diffuser			*Design operating point*		
Number of vanes	Z_d	9	Flow rate	Q_{des}	0.0045 m^3/s
Inlet radius	R_3	77.5 mm	Rotating speed	n_{des}	1450 rpm
Outlet radius	R_4	95 mm	Delivery head	H_{des}	7 m
Vane height	b_d	14 mm	Specific speed	n_q	22.6 (rpm, m^3/s, m)

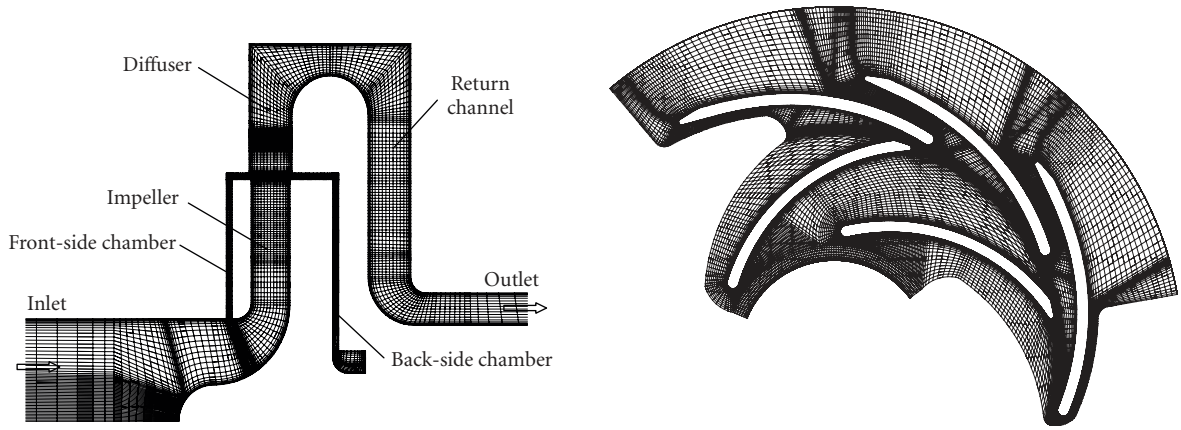

(a) In a meridional plane

(b) At midspan

Figure 1: Grid view of the computational domain.

4 mm for the convenience of PIV and LDV measurements. The specifications of the pump stage are illustrated in Table 1 in detail.

The structured grid for computational domains, shown in a meridional plane and at the midspan of the impeller and diffuser in Figure 1, is created in three parts by using the commercial software ICEM-CFD [15] with multiblock templates: the impeller, diffuser, and return channel respectively. For each part, the template automatically defines a periodic connection between the two lateral sides of the grid; therefore only one blade passage needs meshing. The grid for other blade passages can be obtained by rotation around the rotating axis of the pump directly with the guarantee of one-to-one connection between two periodic surfaces. For the impeller, the side chambers are also included in the grid generation to take leakage flow effects into account. The first grid node from the wall is well controlled in the grid generation process to make $y+$, the dimensionless distance between the first node and the wall, below 60 in the whole computational domains, which enables better resolutions on the boundary layer by the wall functions. The detailed grid information is given in Table 2.

3. UNSTEADY CALCULATION SETUP

Only one third of the pump stage is simulated with periodic conditions because the blade number ratio is 6 (impeller) : 9 (diffuser) : 9 (return channel), which can be simplified to 2 : 3 : 3 under guarantee of pitch ratio of unity. In this case, the total number of nodes is about 1.7 million. The expected periodicity of the flow field has been validated in our previous work [16].

Three-dimensional, unsteady Reynolds-averaged Navier-Stokes equations are solved by the CFD code CFX-10. For boundary conditions, the total pressure and flow direction are imposed at the inlet, and the mass flow rate is given at the outlet. A no-slip wall condition is specified for the flow at the wall boundaries of the hubs, the shrouds, the blades and the vanes, and also the upper and lower surfaces of the side chambers. The boundary condition for the axial end of

Table 2: Grid information.

Region		Blocks	Hexahedral elements	Nodes
Impeller (two passages)	Main part	52	498 432	525 007
	Front-side chamber	24	128 256	141 664
	Back-side chamber	20	113 664	126 400
Diffuser (three passages)		129	477 942	519 611
Return channel (three passages)		126	367 200	395 157
Sum		351	1 585 494	1 707 839

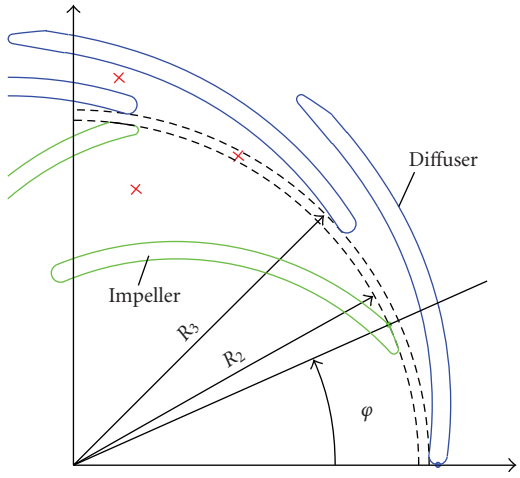

Figure 2: Definition of rotating angle.

the impeller back side chamber is chosen to be a wall, due to the side ring sealing there. The turbulence is simulated by the shear stress transport (SST) turbulence model with automatic near wall treatments [17], with 5% turbulence intensity and a viscosity ratio of 10. The discretization in space is of second order accuracy. The second order backward Euler scheme is chosen for the time-dependent terms. The interface between the impeller and the diffuser is set to "transient rotor-stator," in which the relative position between the rotor and the stator is updated each time step. The time step Δt is set to 1.14942×10^{-4} s, corresponding to a rotating angle change of $\Delta\varphi = 1$ deg per time step in the case of the rotating speed of 1450 rpm. The maximum number of iterations for each time step is set to 10 in order to reduce all maximum residuals below 10^{-3}. Concerning the big size of the grid (about 1.7 million), a parallel calculation is performed on a Linux cluster with 16 processors with standard PC components.

The rotating angle φ defined in Figure 2 is used to indicate the impeller angular position from the diffuser leading edge. When $\varphi = 0$ deg, the trailing edge of an impeller blade begins to approach the leading edge of a diffuser vane. When $\varphi = 4$ deg, this approaching process finishes and the impeller blade trailing edge is positioned closest to the diffuser vane leading edge. In addition, monitor points at midspan marked in red crosshairs are set to monitor unsteady pressures during the unsteady calculations.

4. RESULTS

For each case, a periodic flow field is considered to achieve judged by the pressure fluctuations on the monitor points. After that, one more impeller revolution is calculated further to get transient statistics of the results, in which the maxima, minima, time averages, and standard deviations of the pressure and velocity on each grid node in the computational domains are recorded. Instantaneous pressure on a grid node can be decomposed into two parts: the time-averaged pressure $\overline{p}$ in (1) and the fluctuating pressure $\widetilde{p}$ in (2) representing the part of the pressure changing periodically with the blade passing frequency. To determine the magnitude of pressure fluctuation, we define a nondimensional pressure coefficient $(C_p)_{\text{sdv}}$ in (3), which is calculated by the standard deviation of unsteady pressures normalized by the dynamic pressure based on the impeller tip speed U_2,

$$\overline{p}(\text{node}) = \frac{1}{N}\sum_{j=0}^{N-1} p(\text{node}, t_0 + j\Delta t), \tag{1}$$

$$\widetilde{p}(\text{node}, t) = p(\text{node}, t) - \overline{p}(\text{node}), \tag{2}$$

$$(C_p)_{\text{sdv}} = \frac{\sqrt{(1/N)\sum_{j=0}^{N-1} \widetilde{p}(\text{node}, t_0 + j\Delta t)^2}}{0.5\rho U_2^2}, \tag{3}$$

where N is the sample number during one period, that is, the number of time steps in one period; t_0 is the time to start the statistics.

4.1. Characteristic curve of the pump stage

The comparison between the head characteristics obtained by numerical simulations and experiments is shown in Figure 3. During the numerical simulations, the delivery head is obtained by averaging the head during one impeller revolution since it is fluctuating with the relative impeller position. Obviously, the agreement between them is quite good. Although the result obtained by numerical simulation is somewhat higher than that by the experiment in the whole flow rate range, the biggest relative difference is 3%, occurring at the lowest flow rate ($Q/Q_{\text{des}} = 0.5$). The best agreement between the numerical and experimental results is observed at Q_{des}, and the agreement at over flow operating points is better than at part flow operating points.

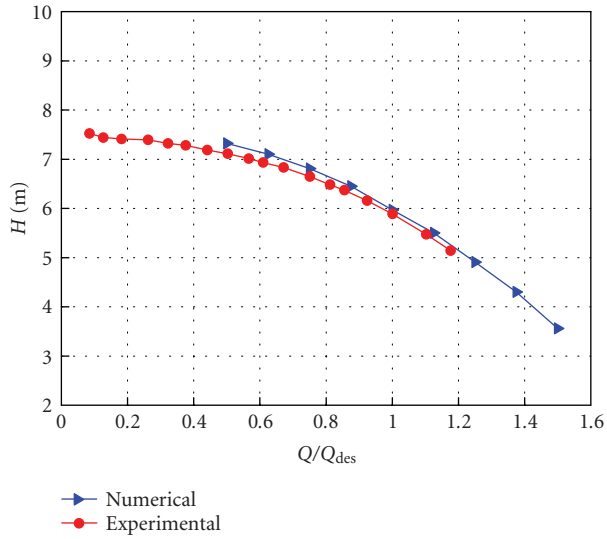

Figure 3: Characteristic curve.

4.2. Results at design operating point Q_{des}

Figure 4 shows the instantaneous radial and circumferential velocity distributions at the impeller outlet at midspan for two different relative positions between the impeller and diffuser. For clarity, the circumferential positions of the impeller blades and diffuser vanes are marked at the top and bottom of the figure, respectively. In the vicinity of each diffuser leading edge, a local minimum of radial velocity could be observed, indicating the potential effect from the impeller-diffuser interactions. The radial velocity reaches a peak near pressure side of the impeller passage, and it goes down to a local minimum on the suction side of the passage, which is very evident in the averaged distribution. This is so called jet-wake flow structure. For the circumferential velocity component, it reaches a peak near the pressure side of the impeller passage, and the peak-to-peak difference is 45% of U_2. Therefore, the velocity components strongly depend on the impeller relative position to the diffuser.

The blade-to-blade distribution of pressure fluctuation at midspan of the impeller is plotted in Figure 5. The pressure fluctuation exhibits a good periodicity between two impeller channels. In general, the fluctuation increases with increasing radius, and the biggest one occurs at the impeller outlet. The biggest pressure fluctuation on the impeller blade is observed at the trailing edge and on the pressure side near the trailing edge, reaching up to 0.065, corresponding to 7.3% of the total head rise in the pump stage. The high pressure fluctuation is reflected upstream to the impeller inlet with decreasing amplitude. On the front half of the impeller blade, the amplitude is increasing slowly, especially on the suction side. Note that there is a small region in the middle chord of the impeller pressure side where the pressure fluctuation decreases slightly when the radius increases. It is also found that the pressure fluctuation on the pressure side of the impeller is much bigger than on the suction side for a given radius, which has also been found experimentally by Arndt et al. [10, 11] and numerically by Shi and Tsukamoto [9], and this trend becomes more evident at the rear part of the impeller blade. The reason is that the interactions between the impeller trailing edge and diffuser leading edge are reflected directly on the impeller pressure surface rather than on the suction surface due to the blade geometry, that is, the impeller pressure side is more exposed to the unsteady interactions than the suction side.

Figure 6 illustrates the pressure fluctuation in the diffuser region. It can be observed that the highest one occurs at the leading edge corresponding to the stagnation point, reaching up to 0.11, which is bigger than the highest one in the impeller region. The diffuser region can be divided into three parts: the full vaned zone, the semivaned zone on the pressure side, and the semivaned zone on the suction side. In the fully vaned zone, the pressure fluctuation decreases with increasing radius, and it decays very fast, resulting in smaller pressure fluctuation in the semivaned zone on the pressure side. However, the one on the semivaned zone on the suction side is quite complicated. First, the pressure fluctuation decreases when the radius increases. This is normal that the unsteady effects decay as the radial distance to the gap region increases. When moving further along the semivaned zone on the suction side, the pressure fluctuation increases due to the adjacent leading edge effects. The leading edge holds the biggest pressure fluctuation and the diffuser passage width is nearly in the same order of the blade thickness. Therefore, the high-pressure fluctuation around the leading edge traverses to the adjacent suction side with decaying magnitude but still remarkable.

4.3. Flow rate effects

The flow rate effects on the unsteady flow can be examined by comparing the results obtained at different flow rates. For this purpose, the simulations are conducted for this pump stage at two other operating points: a part flow operating point ($Q/Q_{des} = 0.5$) and an over flow operating point ($Q/Q_{des} = 1.25$), respectively.

Figure 7 shows the flow rate effects on the pressure fluctuation on the impeller blade. For all flow rates, the biggest pressure fluctuation on the impeller blade is observed at the trailing edge and on the pressure side near the trailing edge. Furthermore, the pressure fluctuation on the pressure side is bigger than on the suction side generally. It seems that the flow rate has a significant effect on the pressure fluctuation. It is found that the amplitude of pressure fluctuation increases significantly with decreasing flow rate, and this trend becomes more evident at the rear part of the impeller blade. For the flow rate $Q/Q_{des} = 0.5$, the biggest one is twice bigger than that for $Q/Q_{des} = 1$. Moreover, the impeller pressure side is more influenced by the flow rate, resulting in a bigger change in the amplitude of pressure fluctuation compared to the impeller suction side. When the flow rate is reduced greatly to $Q/Q_{des} = 0.5$, different types of unsteady flow patterns can be observed, such as flow separation on the impeller suction side (Figure 8).

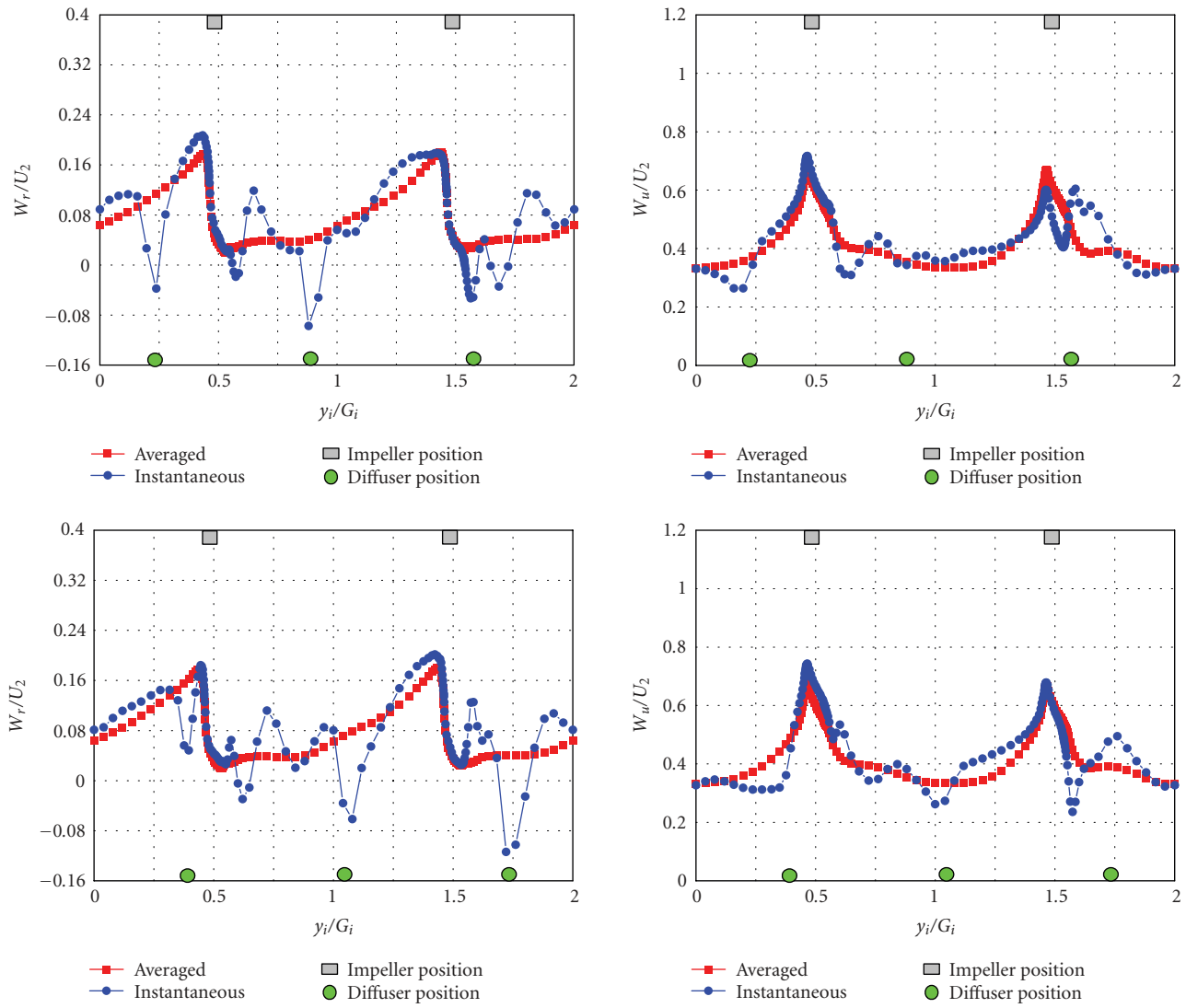

FIGURE 4: Relative radial and circumferential velocity profiles at the impeller outlet ($R/R_2 = 1.01$) at midspan Q_{des}.

Figure 9 shows the flow rate effects on the pressure fluctuation on the diffuser vane surface at midspan. Decreasing the flow rate to $Q/Q_{des} = 0.5$ increases significantly the pressure fluctuation on the whole pressure side, around the leading edge and on the suction side behind the relative chord of 0.3. Increasing the flow rate to $Q/Q_{des} = 1.25$ only results in a slight increase in pressure fluctuation. Therefore, the design operation point Q_{des}, that is, the best match point between the impeller and the diffuser, has the smallest pressure fluctuation on the diffuser vane surface.

4.4. Radial gap effects

The radial gap between the impeller outlet and diffuser vane inlet has been reported to be an important factor to the unsteady phenomena. Some research has been conducted to study the radial gap effects to unsteady flow in the diffuser region. For example, Arndt et al. [11] measured the pressure fluctuations in the diffuser region with two different radial gaps. Qin and Tsukamoto [18] studied the gap effect on pressure fluctuations in the diffuser region by a two-dimensional inviscid simulation. To study the radial gap effects on the impeller here, the radial gap between the impeller and diffuser is increased from 3% to 10% of the impeller outlet radius by moving the diffuser inlet from 77.5 mm to 82.8 mm along the centerline direction of the vane while keeping the outlet radius unchanged. The calculations are performed at the design operating point Q_{des} and the obtained results between two radial gaps are compared in the following section.

The pressure fluctuations on the impeller blade surface are plotted for both gaps at midspan in Figure 10. It is rather evident that increasing radial gap results in a significant reduction in the amplitude of pressure fluctuation, and this trend is more evident in the rear part of the impeller blade, suggesting that the nonuniformity in the circumferential direction of the impeller is quite smaller for the bigger radial

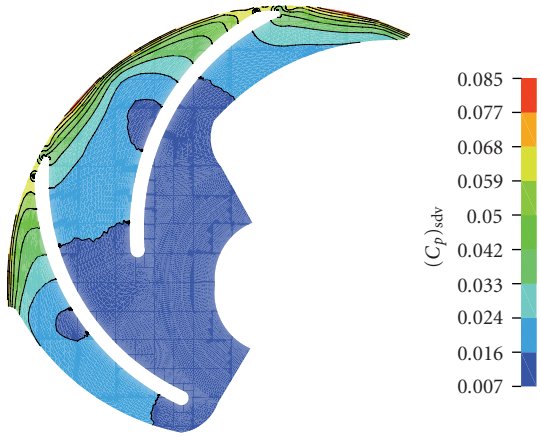

Figure 5: Pressure fluctuation in the impeller at midspan Q_{des}.

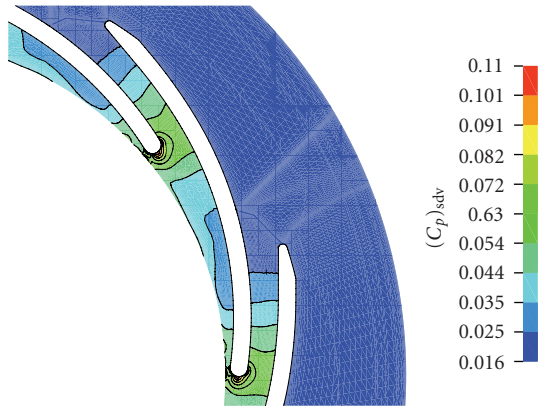

Figure 6: Pressure fluctuation in the diffuser at midspan Q_{des}.

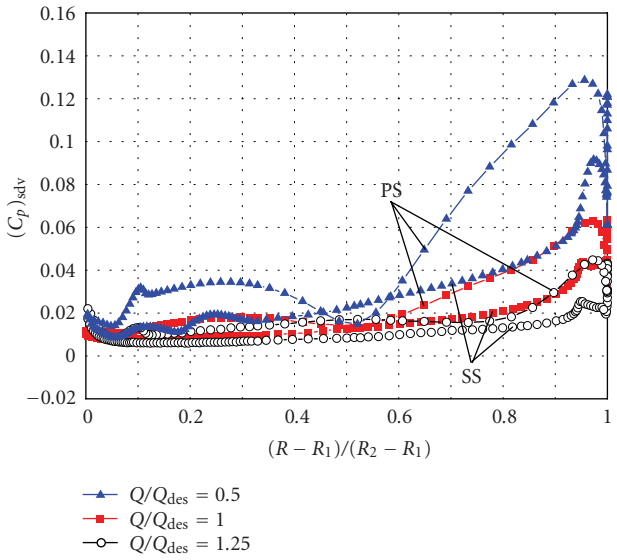

Figure 7: Comparison of pressure fluctuation on the impeller blade, midspan.

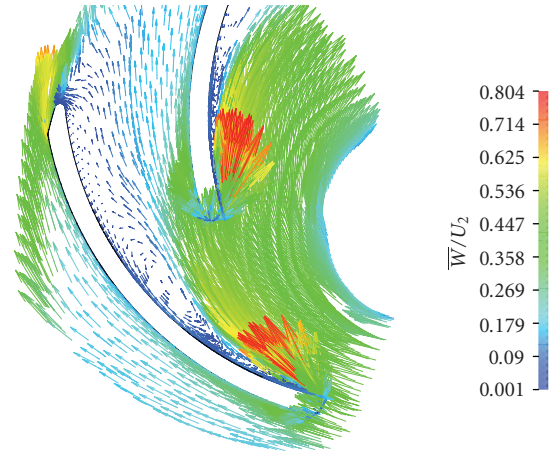

Figure 8: Time-averaged relative vector in the impeller, midspan, 0.5 Q_{des}.

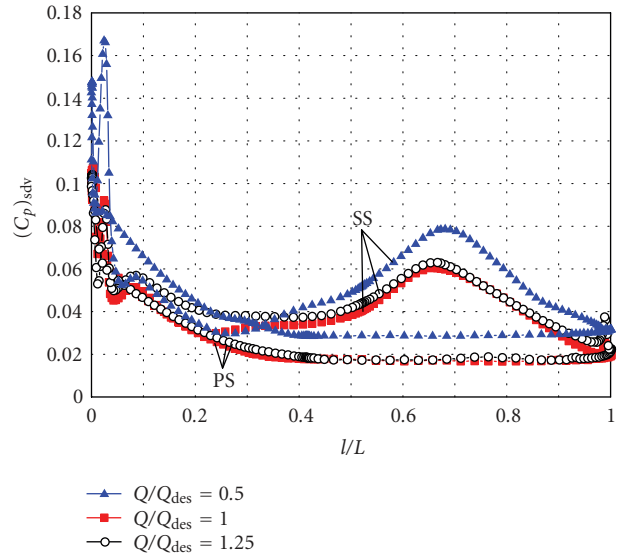

Figure 9: Comparison of pressure fluctuation on the diffuser vane, midspan.

gap. Moreover, the gap influence on the pressure fluctuation is bigger on the impeller blade pressure side than on the suction side due to the fact that the pressure side is more exposed to the interactions. When comparing the arithmetic average of the pressure fluctuation coefficient on the whole impeller blade surface, the increase in radial gap reduces greatly the fluctuation by over 60% (from 0.022 to 0.0083).

The comparison of total force on a single impeller blade between two radial gaps is shown in Figure 11. The force is calculated using momentum flow data in the result, including pressure and viscous forces. It is found that the pressure force is more than two orders of magnitude greater than the viscous force. For both cases, the force exhibits a good periodicity for each diffuser vane circumferential pitch. When the suction side of an impeller trailing edge approaches a

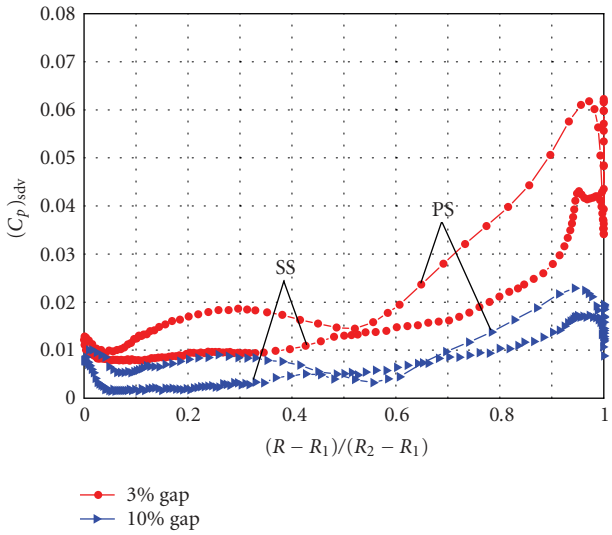

Figure 10: Pressure fluctuations on the impeller blade for two gaps at middle span.

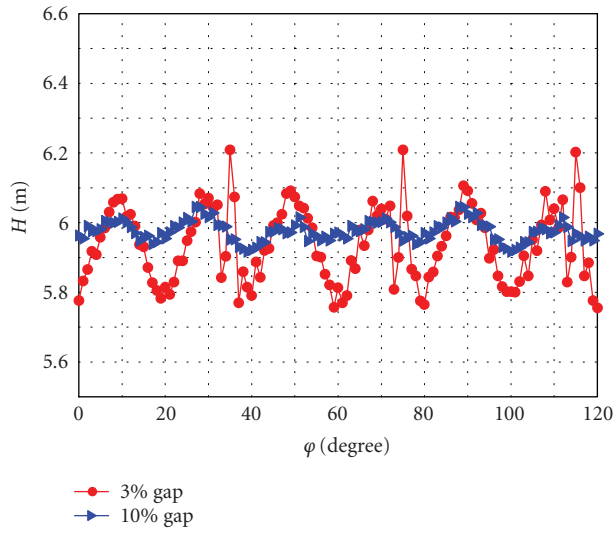

Figure 12: Delivery head fluctuation.

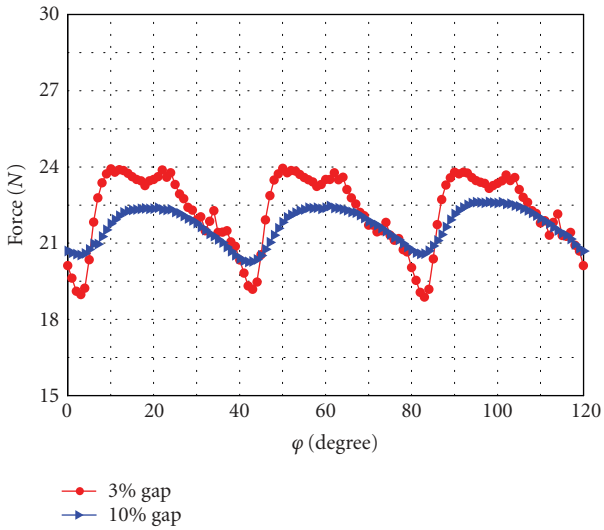

Figure 11: Total force on the impeller blade.

diffuser vane leading edge ($\varphi = 4°, 44°, 84°$), the total forces for both radial gaps attain local minima. Concerning the gap effects, the force curve of 10% gap is much smoother than that of 3% gap. Although there is no big difference in the time-averaged force (22.3 N for 3% gap and 21.6 N for 10% gap), the peak-to-peak difference during one impeller revolution for 3% gap is about twice bigger than that for 10% gap.

Figure 12 illustrates the comparison of delivery head between two radial gaps. It can be observed that the head curve of 3% gap has a much stronger fluctuation than that of 10% gap, and the peak-to-peak difference of delivery head in one impeller revolution for 3% gap is nearly three times bigger than that for 10% gap. The predicted curve for 10% gap is also much smoother than that for 3% gap, showing that the unsteady interaction is much weaker than that of 3% gap.

4.5. Blade number configuration effects

In this part, several pump configurations in the variation of impeller and diffuser blade numbers are studied. Two more configurations are considered here: (1) reducing the diffuser vane number from nine to seven, indicated as 6I7D9R (6 impeller blades, 7 diffuser vanes, and 9 return channel vanes); (2) increasing the impeller blade number from six to nine, indicated as 9I9D9R. The original one is denoted by 6I9D9R. All calculations here are performed only at the design operating point Q_{des} for comparison. For the case of 9I9D9R, the simulation is conducted for one blade channel for each component; but for 6I7D9R, the simulation is performed for all blade channels since there is no common factor except one between the blade numbers.

The pressure fluctuations on an impeller blade surface are compared at midspan in Figure 13 for different blade configurations. It can be noted that the decrease of the diffuser vane number from nine to seven leads to an increase in pressure fluctuation in the whole range due to the increasing nonuniformity in the circumferential direction at the impeller outlet during one impeller revolution. When increasing the number of impeller blades from six to nine, resulting in an identical number as the diffuser vanes, the pressure fluctuation on the impeller suction side on the rear part decreases slightly; however, the one on the impeller pressure side on the rear half part increases greatly.

The comparison of total force acted on a single impeller blade is given in Figure 14. A similar trend can be found: the force on the blade decreases to a local minimum when the suction side of the impeller trailing edge approaches a diffuser leading edge, then it increases to a peak with a great gradient. The decrease in diffuser vane number from nine to

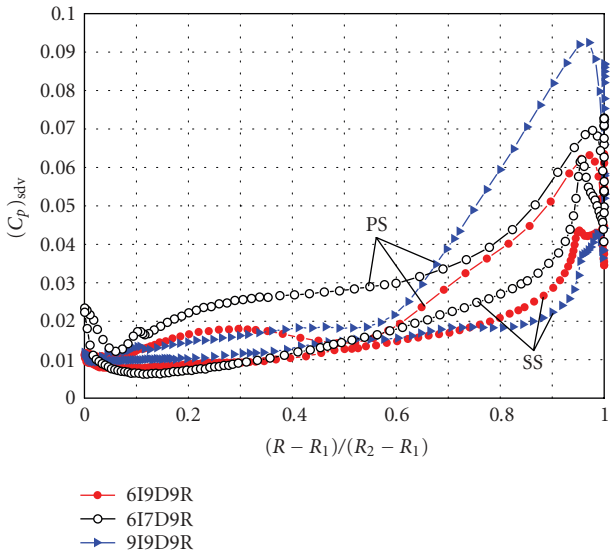

Figure 13: Comparison of pressure fluctuation on the impeller blade for three blade number configurations, midspan.

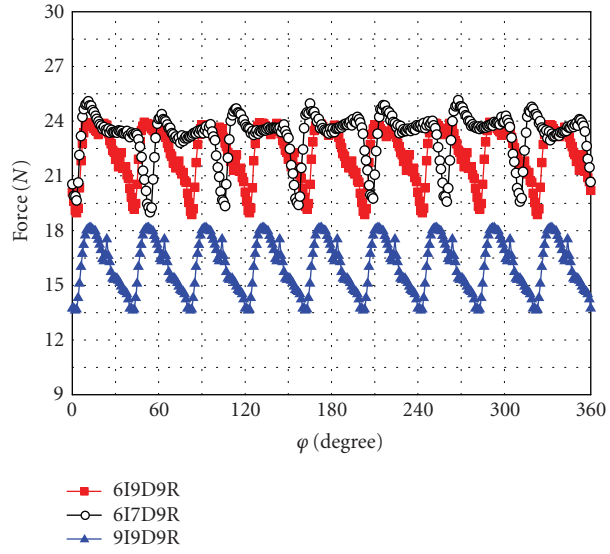

Figure 14: Comparison of total force on a single impeller blade for three blade number configurations, midspan.

seven brings a slight increase on the magnitude of the impeller blade force. When increasing the impeller blade number from six to nine, it results in a significant reduction in the force level due to the reducing loading on a single blade. However, the fluctuating amplitude (peak-to-peak difference) of the force does not decrease because of the bigger pressure fluctuation at the rear part of the impeller blade occurring when the impeller and diffuser have the same blade number.

Figure 15 plots the pressure fluctuations in the diffuser region at midspan for all three blade configurations with the same scale. All cases predict a region on the semi-vaned zone suction side with local smaller pressure fluctuation, and a high-pressure fluctuation region around the diffuser leading edge. Decreasing the number of diffuser vanes from nine to seven results in a slight increase of pressure fluctuation around the diffuser trailing edge. For the case with identical blade number between the impeller and diffuser, the pressure fluctuation is observed to be the largest in all three cases on the whole diffuser vane surface. In addition, the pressure fluctuation does not decay after the diffuser throat as that occurs in the other two cases, and the fluctuation keeps nearly constant in high amplitude after the outlet throat. This high pressure fluctuation is transferred downstream of the diffuser, responsible for a higher amplitude of the delivery head fluctuation.

The total forces on a single diffuser vane are compared among different blade configurations in Figure 16. The original configuration has the smallest force on the vane surface. Decreasing the number of diffuser vanes results in an increase of the loading on a single diffuser vane. Consequently, the force on a single diffuser vane also increases. Increasing the number of impeller blades to the same number of the diffuser vanes leads to an increase in the averaged force on a single diffuser vane, especially in the peak force.

4.6. *Time-step independent research*

The influence of time step for the unsteady simulations on the numerical results is presented for the original pump configuration at the design operating point in Figure 17, in which the instantaneous pressures at three monitor points (Figure 2), one is in the impeller region, one is in the diffuser region, and one is in the radial gap region between the impeller and diffuser, are compared during one impeller revolution for two different time steps chosen for the transient simulations. It can be seen that decreasing the time step by a factor of two has nearly no influence on the pressures for all monitor points. Thus, the selected time step 1.14942×10^{-4} s is assumed to be small enough to get a time-step independent result.

5. CONCLUSIONS

Numerical simulations are performed in CFX-10 to investigate the unsteady flow, especially the pressure fluctuation in radial diffuser pumps. Calculations are performed at different operating points, radial gaps, and blade number configurations between the impeller and diffuser. The computational results show the following.

(1) A jet-wake flow structure is found at the impeller outlet.
(2) The pressure fluctuation on the impeller pressure side is much bigger than on the impeller suction side, and it is more evident at the rear part of the impeller blade.
(3) The biggest pressure fluctuation on the impeller blade is observed at the trailing edge and on the pressure side near the trailing edge; for the diffuser vane, it is at the vane leading edge, independent of the flow rate and blade number configuration.

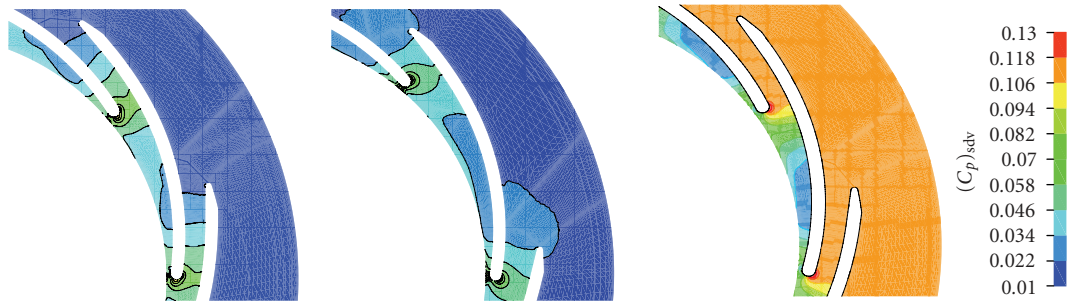

(a) $Z_i = 6, Z_d = 9, Z_r = 9$ (b) $Z_i = 6, Z_d = 7, Z_r = 9$ (c) $Z_i = 9, Z_d = 9, Z_r = 9$

Figure 15: Pressure fluctuation in the diffuser region, midspan.

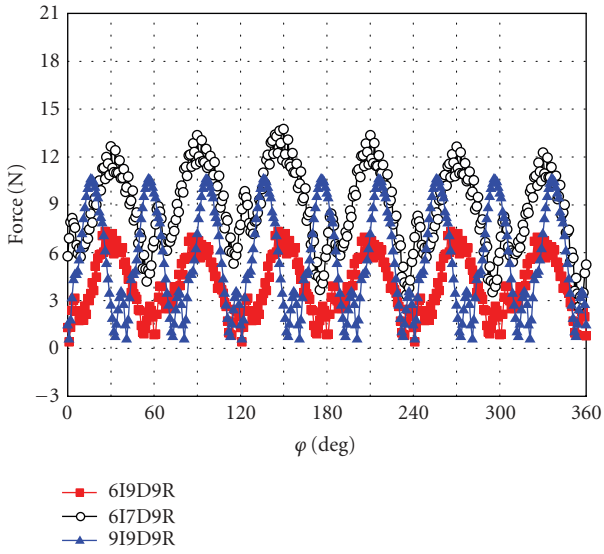

Figure 16: Total force on a single diffuser vane.

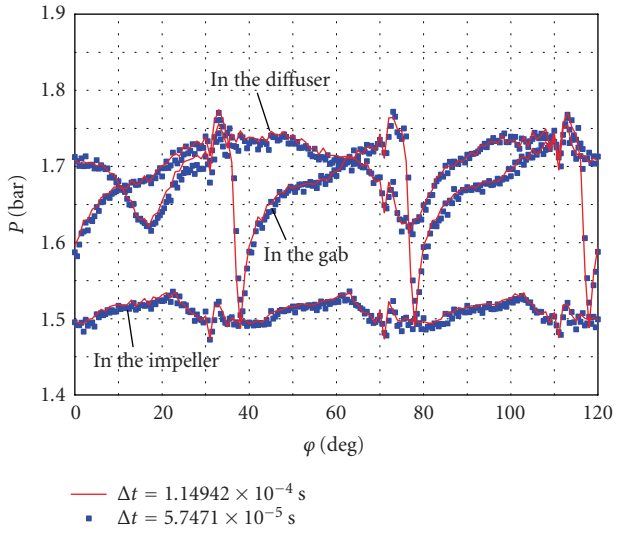

Figure 17: Time-step effects on unsteady pressures.

(4) The pressure fluctuation in the impeller increases significantly with decreasing mass flow rate. For the diffuser vane, the smallest pressure fluctuation occurs at the design operating point.
(5) Increasing the radial gap from 3% to 10% results in a reduction of over 60% in the amplitude of the pressure fluctuation on the impeller blade surface, indicating that the impeller-diffuser interactions are significantly weakened. In addition, the gap influence on the pressure fluctuation is bigger on the impeller blade pressure side than on the impeller suction side.
(6) Decreasing the number of diffuser vanes from nine to seven leads to an increase in pressure fluctuation on the impeller blade surface and a slight increase around the diffuser vane trailing edge. The force on a single impeller blade is reduced slightly, but the force on a single diffuser vane is increased.
(7) Increasing the number of the impeller blades from six to nine, the same number as the diffuser vanes, leads to an increase of pressure fluctuation on the impeller pressure side and on the whole diffuser vane surface; the pressure fluctuation does not decay but keeps high amplitude after the diffuser throat. The force on a single impeller blade decreases greatly but still in high fluctuating amplitude. It also leads to an increase in the averaged force on a single diffuser vane, especially in the peak force.

Nomenclature

b: Blade height
g: Acceleration due to gravity
G: Circumferential pitch
h: Height
l: Chord coordinate
L: Chord length
n: Rotating speed
n_q: Specific speed
p: Static pressure
p_{tot}: Total pressure
Q: Volume flow rate
R: Radius

U: Circumferential velocity
W: Relative velocity
W_r: Relative radial velocity
W_u: Relative circumferential velocity
y: Circumferential coordinate
φ: Rotating angle
PS: Pressure side
SS: Suction side
$(C_p)_{\mathrm{sdv}}$: Pressure fluctuation coefficient
$H = \overline{P_{\mathrm{tot}}^{\mathrm{outlet}}} - \overline{P_{\mathrm{tot}}^{\mathrm{inlet}}}/\rho g$: Delivery head
Δt: Time step
ρ: Density of water

Subscripts

bs: Back-side chamber
d: Diffuser
fs: Front-side chamber
i: Impeller
r: Return channel
sdv: Standard deviation
1: Impeller inlet
2: Impeller outlet
3: Diffuser inlet
4: Diffuser outlet
5: Return channel inlet
6: Return channel outlet

Superscripts

– Time-averaged
$\sim$ Fluctuating

REFERENCES

[1] M. El Hajem, A. Akhras, R. Morel, and J.-Y. Champagne, "Rotor stator interaction in a centrifugal pump equipped with a vaned diffuser," in *Proceedings of the 4th European Conference on Turbomachinery, Fluid Dynamics and Thermodynamics*, Firenze, Italy, March 2001.

[2] A. Akhras, M. El Hajem, J.-Y. Champagne, and R. Morel, "The flow rate influence on the interaction of a radial pump impeller and the diffuser," *International Journal of Rotating Machinery*, vol. 10, no. 4, pp. 309–317, 2004.

[3] M. Sinha and J. Katz, "Quantitative visualization of the flow in a centrifugal pump with diffuser vanes—I: on flow structures and turbulence," *Journal of Fluids Engineering*, vol. 122, no. 1, pp. 97–107, 2000.

[4] M. Sinha, J. Katz, and C. Meneveau, "Quantitative visualization of the flow in a centrifugal pump with diffuser vanes—II: addressing passage-averaged and large-eddy simulation modeling issues in turbomachinery flows," *Journal of Fluids Engineering*, vol. 122, no. 1, pp. 108–116, 2000.

[5] G. Wuibaut, G. Bois, P. Dupont, G. Caignaert, and M. Stanislas, "PIV measurements in the impeller and the vaneless diffuser of a radial flow pump in design and off-design operating conditions," *Journal of Fluids Engineering*, vol. 124, no. 3, pp. 791–797, 2002.

[6] W. Qin and H. Tsukamoto, "Theoretical study of pressure fluctuations downstream of a diffuser pump impeller—part 1: fundamental analysis on rotor-stator interaction," *Journal of Fluids Engineering*, vol. 119, no. 3, pp. 647–652, 1997.

[7] H. Wang and H. Tsukamoto, "Fundamental analysis on rotor-stator interaction in a diffuser pump by vortex method," *Journal of Fluids Engineering*, vol. 123, no. 4, pp. 737–747, 2001.

[8] H. Wang and H. Tsukamoto, "Experimental and numerical study of unsteady flow in a diffuser pump at off-design conditions," *Journal of Fluids Engineering*, vol. 125, no. 5, pp. 767–778, 2003.

[9] F. Shi and H. Tsukamoto, "Numerical study of pressure fluctuations caused by impeller-diffuser interaction in a diffuser pump stage," *Journal of Fluids Engineering*, vol. 123, no. 3, pp. 466–474, 2001.

[10] N. Arndt, A. J. Acosta, C. E. Brennen, and T. K. Caughey, "Rotor-stator interaction in a diffuser pump," *Journal of Turbomachinery*, vol. 111, no. 3, pp. 213–221, 1989.

[11] N. Arndt, A. J. Acosta, C. E. Brennen, and T. K. Caughey, "Experimental investigation of rotor-stator interaction in a centrifugal pump with several vaned diffusers," *Journal of Turbomachinery*, vol. 112, no. 1, pp. 98–108, 1990.

[12] A. Furukawa, H. Takahara, T. Nakagawa, and Y. Ono, "Pressure fluctuation in a vaned diffuser downstream from a centrifugal pump impeller," *International Journal of Rotating Machinery*, vol. 9, no. 4, pp. 285–292, 2003.

[13] S. Guo and Y. Maruta, "Experimental investigations on pressure fluctuations and vibration of the impeller in a centrifugal pump with vaned diffusers," *JSME International Journal, Series B: Fluids and Thermal Engineering*, vol. 48, no. 1, pp. 136–143, 2005.

[14] ANSYS, "CFX User Document, version 10.0," ANSYS Europe, 2005.

[15] ANSYS, "ICEM-CFD User Document, version 10.0.1," ANSYS Europe, 2005.

[16] F.-K. Benra, J. Feng, and H. J. Dohmen, "Numerical study on pressure fluctuations in a complete stage of a centrifugal pump," in *Proceedings of the 11th International Symposium on Transport Phenomena and Dynamics of Rotating Machinery (ISROMAC-11 '06)*, Honolulu, Hawaii, USA, February-March 2006.

[17] F. R. Menter, "Two-equation eddy-viscosity turbulence models for engineering applications," *AIAA journal*, vol. 32, no. 8, pp. 1598–1605, 1994.

[18] W. Qin and H. Tsukamoto, "Theoretical study of pressure fluctuations downstream of a diffuser pump impeller—part 2: effects of volute, flow rate and radial gap," *Journal of Fluids Engineering*, vol. 119, no. 3, pp. 653–658, 1997.